Theory of photoabsorption in modulation-doped semiconductor quantum wells

G. D. Sanders* and Yia-Chung Chang
Department of Physics and Materials Research Laboratory, University of Illinois at Urbana-Champaign, 1110 West Green Street, Urbana, Illinois 61801
(Received 1 May 1986; revised manuscript received 11 August 1986)

A systematic study of the electronic and optical properties of modulation-doped GaAs-$Al_xGa_{1-x}As$ quantum wells is undertaken. We consider cases in which the $Al_xGa_{1-x}As$ barriers are doped either n or p type and the GaAs wells are filled with a gas of free carriers. The electronic band structure, exciton binding energy, exciton oscillator strength, and interband absorption are studied as functions of well width and doping concentration. A multiband effective-mass method is used which takes coupling between heavy- and light-hole states into account. In our model for excitons we include effects of valence-subband nonparabolicity, free-carrier screening, and the $\mathbf{k}$ dependence of optical matrix elements. The interband optical absorption is obtained using Fermi's golden rule with a correction made for the screened final-state interaction. Our theoretical results are compared with available experimental data.

I. INTRODUCTION

Modulation-doped GaAs-$Al_xGa_{1-x}As$ semiconductor superlattices and quantum wells have received growing interest in recent years.[1-4] In these systems the $Al_xGa_{1-x}As$ barriers are doped either n or p type and the GaAs wells are filled with a gas of free carriers. Most of the experimental and theoretical work done so far has centered on the study of the transport properties of the free carriers confined in the GaAs wells.[1-4] This interest is primarily due to the fact that extremely high mobilities result from segregation of the free carriers and doping impurities.

Relatively little attention has been paid to optical-absorption properties in these systems although it has been pointed out that the light sensitivity and persistent photoconductive effects in modulation-doped structures have important practical consequences for the construction of modulation-doped field-effect transistors.[5] Recently, photoluminescence, photoexcitation, and absorption measurements have been made on modulation-doped samples.[6-8] In this paper we report on calculations of electronic and optical properties in these systems. We study electronic band structure, exciton binding energy, exciton oscillator strength, and interband absorption and compare our results with the available data.

The remainder of the paper is organized as follows. First, we discuss the electronic and optical properties of the free-electron and hole carrier states. The multiband effective-mass method is described and valence-band structure as functions of well width are discussed. Next electronic properties of exciton states are considered. We describe the exciton effective-mass equation and the exciton screening theory and then discuss exciton wave functions and binding energies as functions of well width and doping level. Optical properties in modulation-doped quantum wells are then discussed. Interband absorption including a correction for the screened final-state interaction and exciton oscillator strengths as functions of doping concentration are described. Finally, a summary and conclusions are presented.

II. ELECTRONIC PROPERTIES OF MODULATION-DOPED QUANTUM WELLS

In our treatment of modulation-doped quantum wells, conduction and valence bands are considered decoupled. This is a good approximation when the fundamental band gap of the well material is much larger than the subband energies of the quantum well. For the conduction-band states, a simple effective-mass theory is used. For the valence-band states, we use a multiband effective-mass theory in which the hole kinetic-energy term is described by a 4×4 matrix whose elements are derived based on the $\mathbf{k}\cdot\mathbf{p}$ method.[9-11] The $\mathbf{k}\cdot\mathbf{p}$ formalism was extended to the study of thin films by Nedorezov,[12] and recently has been used in the study of quantum-well structures.[13-15] For simplicity, the effective masses of electrons and holes in the barrier material ($Al_xGa_{1-x}As$) are assumed to be the same as those in GaAs. The approximation is good as long as the leaking of quantum-well-state wave functions into the barrier is sufficiently small.

The effective-mass Hamiltonian for the spin-$\frac{1}{2}$ conduction-band electron is given by a scalar operator

$$H_e = p^2/2m_e^* + V_e(z) - V_d(z) , \tag{1}$$

where m_e^* is the effective electron mass for GaAs, $V_e(z)$ is a finite square-well potential of depth V_{0e}, and $V_d(z)$ is an additional parabolic potential of height V_0 which models the effects of modulation doping. Throughout the paper, the z axis is taken to be along the growth direction of the quantum well.

The square-well potentials arise as a result of the band-gap mismatch between GaAs and $Al_xGa_{1-x}As$ which we take to be $\Delta E_g = (1.115x + 0.37x^2)$ eV.[16] This band-gap mismatch is divided between the conduction and valence bands to form the confining potentials, and thus $V_e(z)$

has a height $Q_e\Delta E_g$ and $V_h(z)$ has a height $Q_h\Delta E_g=(1-Q_e)\Delta E_g$. The band offset parameters Q_e and Q_h are taken to be 0.6 and 0.4, respectively,[17] and for the Luttinger parameters of GaAs we adopt values of $\gamma_1=6.85$, $\gamma_2=2.1$, and $\gamma_3=2.9$.[18]

The relation between the height of the parabolic potential (V_0) and the two-dimensional carrier concentration is given by[19]

$$N=(1/4\pi e^2)(8\epsilon\,|\,V_0\,|\,/W)$$

where ϵ is the static dielectric constant of the well material, W is the well width, and e is the electric charge of the carrier. This approximation is valid as long as V_0 is reasonably weak ($\lesssim 10$ meV). In our formalism V_0 is positive for p-type modulation-doped quantum wells and negative for n type. The parabolic potential approximation is equivalent to the assumption that there is a uniform density of carriers in the well. Examination of the calculated ground-state wave function for the case where only one subband is occupied shows that the assumption of uniform carrier density is adequate for quantum wells having widths in the range 50—200 Å. If we generate an improved potential based on our calculated wave functions it is seen to be approximately parabolic and to deviate from the original potential by at most 20%. Using first-order perturbation theory, it can be shown that the deviation between the two potentials will cause a shift in the subband energy levels of approximately 10% of V_0. The effect on calculated transition energies is smaller still since the errors in the conduction- and valence-subband energies have the same sign and tend to cancel when differences are taken between energy levels.

The effective-mass Hamiltonian for the spin-$\frac{3}{2}$ hole in the limit of infinite spin-orbit coupling is a 4×4 matrix operator given by

$$H_{\nu\nu'}=T_{\nu\nu'}+[V_h(z)+V_d(z)]\delta_{\nu\nu'}\ , \tag{2}$$

where $V_h(z)$ is a finite square well of height V_{0h}, $V_d(z)$ is the aforementioned modulation-doping potential, and ν labels the z component of hole spin, i.e., $\nu\equiv J_z=-\frac{3}{2}$, $-\frac{1}{2}$, $\frac{1}{2}$, $\frac{3}{2}$. $T_{\nu\nu'}$ is the Kohn-Luttinger Hamiltonian.[9]

In the envelope-function approximation we have

$$\psi^e_{n,\mathbf{k}_{||}}(\rho,z)=\sum_\sigma e^{i\mathbf{k}_{||}\cdot\rho}f^\sigma_n(\mathbf{k}_{||},z)\,|\,\psi^e_\sigma\rangle \quad \text{for electrons} \tag{3}$$

and

$$\psi^h_{m,\mathbf{k}_{||}}(\rho,z)=\sum_\nu e^{i\mathbf{k}_{||}\cdot\rho}g^\nu_m(\mathbf{k}_{||},z)\,|\,\psi^h_\nu\rangle \quad \text{for holes}\ , \tag{4}$$

where f^σ_n and g^ν_m are the envelope function, $|\,\psi^e_\sigma\rangle$ and $|\,\psi^h_\nu\rangle$ are bulk Bloch functions at the zone center, and $\mathbf{k}_{||}=k_x\hat{\mathbf{x}}+k_y\hat{\mathbf{y}}$ and $\rho=x\hat{\mathbf{x}}+y\hat{\mathbf{y}}$.

The envelope function and subband structure for valence subbands are obtained by solving the effective-mass equation:

$$\sum_{\nu'}H_{\nu\nu'}(\mathbf{k}_{||})g^{\nu'}_m(\mathbf{k}_{||},z)=E_m(\mathbf{k}_{||})\ . \tag{5}$$

In our multiband effective-mass approach the effective-mass equation for the subband energies and envelope functions $g^\nu_m(\mathbf{k}_{||},z)$ are solved variationally by expanding $g^\nu_m(\mathbf{k}_{||},z)$ as a sum of Gaussian-type orbitals of the form $e^{-\beta z^2}$ and $ze^{-\beta z^2}$. Fifteen Gaussian orbitals of each type are used in our calculation. Substituting this expansion for the envelope functions into the effective-mass equation, the problem reduces to a generalized Hermitian eigenvalue problem to be solved for the subband energies $E_m(\mathbf{k}_{||})$ and the envelope-function expansion coefficients.

The results of our valence-subband calculation in the absence of modulation doping are shown in Fig. 1 for GaAs-$Al_{0.25}Ga_{0.75}As$ quantum wells having well widths of 20, 50, 100, and 200 Å. The valence-subband structure is seen to be very complicated and some of the bands are seen to have negative zone center effective masses. This complicated structure is the result of strong interactions between different subbands due solely to the mixing of heavy- and light-hole states at nonzero values of $\mathbf{k}_{||}$ by the off-diagonal terms in $H_{\nu\nu'}$. At points away from the zone center the increasing strength of the level repulsion interaction between subband states with increasing $\mathbf{k}_{||}$ gives rise to the complicated band structure. In particular, the increasing strength of the level repulsion interaction between LH1 and HH2 gives rise to the negative zone center LH1 effective mass. In the absence of coupling by the off-diagonal terms in $H_{\nu\nu'}$ the subbands would all be parabolas. At the zone center the off-diagonal terms in $H_{\nu\nu'}$ vanish and the heavy- and light-hole states are uncoupled. Thus the $\mathbf{k}_{||}=0$ states can be labeled LHn or HHn for the nth light- or heavy-hole state.

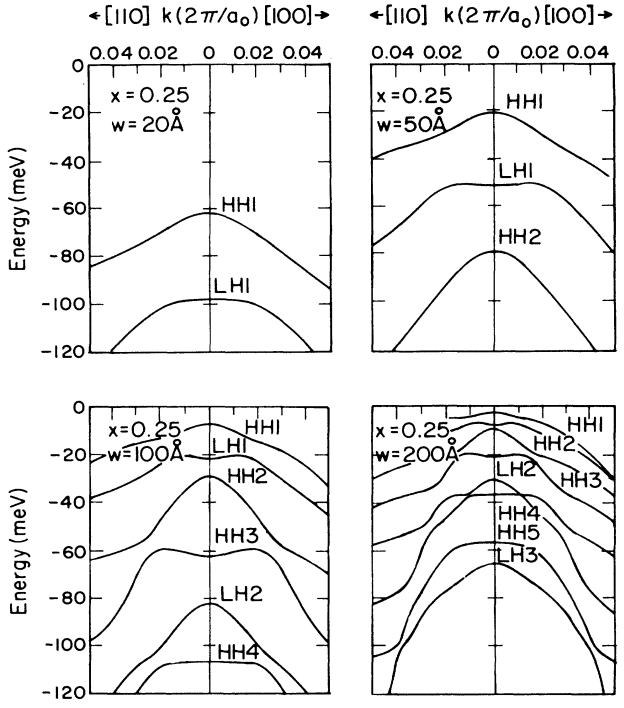

FIG. 1. Valence-subband structure calculated using the multiband effective-mass method for GaAs-$Al_{0.25}Ga_{0.75}As$ quantum wells having thicknesses of 20, 50, 100, and 200 Å.

Similar valence-band structures for undoped GaAs-$Al_xGa_{1-x}As$ quantum wells have previously been reported.[13,14] We have previously reported the effect of modulation doping on the valence-band structures.[14] We found that the valence-band structures are shifted almost rigidly under the influence of the doping potential V_d.

It is instructive to examine the hole envelope wave functions. In Fig. 2 the charge density as a function of z is shown for the HH1 and LH1 variational envelope functions for a 100-Å GaAs-$Al_{0.25}Ga_{0.75}As$ quantum well at the zone center and at $\mathbf{k}_{||}=0.02(2\pi/a)(1,0,0)$. The various envelope-function components are labeled by the spin indices ν in the figure. At the zone center the envelope functions are pure HH1 and LH1 states, while at a point slightly removed from the zone center strong mixing of heavy- and light-hole components is evident. The degree of mixing is determined by the proximity of adjacent states. For example, the HH1 valence-band state at $\mathbf{k}_{||}=0.02(2\pi/a)(1,0,0)$ is primarily $J_z=\frac{3}{2}$ in character with a smaller admixture of $J_z=-\frac{1}{2}$, whereas for the LH1 valence-band state there is strong mixing of the $J_z=\frac{1}{2}$ component with both the $J_z=-\frac{3}{2}$ and $J_z=\frac{3}{2}$ components.

III. EXCITONS IN MODULATION-DOPED QUANTUM WELLS

In recent years GaAs-$Al_xGa_{1-x}As$ superlattices and quantum wells have been extensively studied both experimentally and theoretically, and it is known that excitons play an important role in optical absorption in these systems.[20,21]

Greene and Bajaj have studied free-exciton binding energies in GaAs-$Al_xGa_{1-x}As$ quantum wells in a two-band effective-mass model where the light- and heavy-hole subbands are decoupled and the effective masses in GaAs and $Al_xGa_{1-x}As$ are taken to be equal.[22] The method of Greene and Bajaj has recently been extended by Priester, Allen, and Lannoo.[23] These authors consider the effects of effective-mass mismatches between GaAs and $Al_xGa_{1-x}As$ and find significantly enhanced exciton binding energies for well thickness below 100 Å and binding energies essentially identical to those calculated by Greene and Bajaj for thicker wells. Excitons in quantum wells containing degenerate electrons or holes have been studied recently by Kleinman[24] in a simple model.

In this section we present a theoretical calculation of the binding energies of Wannier excitons in GaAs-$Al_xGa_{1-x}As$ quantum wells that takes into account the effects of valence-band hybridization and screening of the Coulomb interaction by free carriers. The valence bands in quantum wells are highly nonparabolic[13-15,25,26] which we take explicitly into account. It has been shown in the preceding section that several of the hole subbands can have negative zone center effective masses. We find that excitons corresponding to these valence subbands have enhanced binding energies due to the reduction in kinetic energy brought about by their large joint density of states.

In our model of the quantum-well excitons, we first solve the free-carrier problem in the envelope-function approximation for electrons and holes separately as discussed previously. The free-electron and hole carrier states interact through the screened Coulomb force to form excitons. The exciton wave function is made up of linear combinations of direct products of quantum-well electron and hole eigenstates,

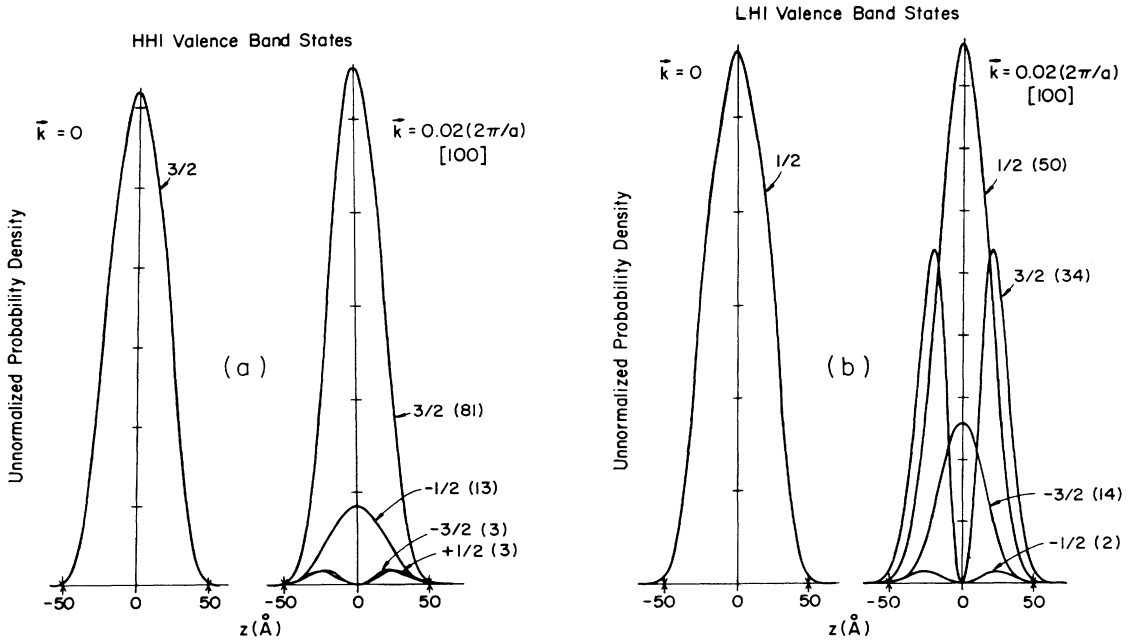

FIG. 2. Charge density as a function of z for a 100-Å GaAs-$Al_{0.25}Ga_{0.75}As$ quantum well at the zone center and at $\mathbf{k}_{||}=0.2(2\pi/a)l$ (1,0,0) for (a) HH1 and (b) LH1 valence-subband states. The numbers in parentheses indicate percentages of total charge density.

$$\psi_x = \sum_{n,m} \sum_{\mathbf{k}_{||}} \sum_{\mathbf{k}'_{||}} F_{nm}(\mathbf{k}_{||},\mathbf{k}'_{||}) \mid \mathbf{k}_{||},n \rangle \mid \mathbf{k}'_{||},m \rangle , \quad (6)$$

where n and m are subband indices for electron and hole, respectively. In the case of modulation doping, either the first conduction subband (for n-type doping) or the first heavy-hole subband (for p-type doping) will be partially filled by carriers. In our calculation, we assume that the exciton state associated with the partially filled subband is a linear combination of single-particle excitations with $\mathbf{k}_{||}$ restricted to regions in $\mathbf{k}_{||}$ space outside the Fermi sphere while keeping all the free carriers in their ground state. In this approximation the polarization of the Fermi sea has been neglected.[27,28] Such a many-body effect will be treated in a separate publication. For excitons associated with unfilled subbands, the theory described here is appropriate and the paper will put more emphases on the carrier screening effect on these excitons. It can be shown that the exciton envelope function satisfies a two-dimensional effective-mass equation. The envelope function is given by

$$F_{nm}(\mathbf{k}_{||},\mathbf{k}'_{||}) = \delta(\mathbf{k}_{||}+\mathbf{k}'_{||}) G_{nm}(\mathbf{k}_{||})$$

where $G_{nm}(\mathbf{k}_{||})$, the exciton relative motion envelope function, satisfies

$$[E_n^e(\mathbf{k}_{||}) - E_m^h(\mathbf{k}_{||})] G_{nm}(\mathbf{k}_{||}) + \sum_{n',m'} \sum_{\mathbf{k}'_{||}} V_{n'm'}^{nm}(\mathbf{k}_{||},\mathbf{k}_{||}) G_{n'm'}(\mathbf{k}'_{||}) = E G_{nm}(\mathbf{k}_{||}) . \quad (7)$$

In this expression $E_n^e(\mathbf{k}_{||})$ and $E_m^h(\mathbf{k}_{||})$ are the energies for the nth conduction and mth valence subbands, and the Coulomb interaction term $V_{n'm'}^{nm}(\mathbf{k}_{||},\mathbf{k}'_{||})$ is given by

$$V_{n'm'}^{nm}(\mathbf{k}_{||},\mathbf{k}'_{||}) = \bar{V}_{n'm'}^{nm}(\mathbf{k}_{||},\mathbf{k}'_{||}) / \epsilon(\mid \mathbf{k}_{||} - \mathbf{k}'_{||} \mid)$$

where $\bar{V}$ is the bare potential which is given by

$$\bar{V}_{n'm'}^{nm}(\mathbf{k}_{||},\mathbf{k}'_{||}) = \frac{e^2}{\epsilon_0 \mid \mathbf{k}_{||} - \mathbf{k}'_{||} \mid} \int \int dz_e \, dz_h \sum_{\sigma} f_{n'}^{*\sigma}(z_e) f_n^{\sigma}(z_e) \sum_{\nu} g_{m'}^{*\nu}(\mathbf{k}'_{||},z_h) g_m^{\nu}(\mathbf{k}_{||},z_h) e^{-\mid \mathbf{k}_{||} - \mathbf{k}'_{||} \mid \mid z_e - z_n \mid} . \quad (8)$$

Here $\epsilon(q_{||})$ is a wave-vector-dependent dielectric function which contains the effects of screening by free carriers which we shall return to shortly and ϵ_0 is the static dielectric constant in GaAs. Derivations of (7) and (8) are given in Appendix B.

We adopt a two-band model keeping only one valence and one conduction subband. We further approximate

$$\sum_{\nu} g_m^{*\nu}(\mathbf{k}'_{||},z_h) g_m^{\nu}(\mathbf{k}_{||},z_h)$$

in (8) by its value at the zone center. This is a fairly good approximation, since the dominating contribution in (8) comes from the $\mathbf{k}_{||} \simeq \mathbf{k}'_{||}$ term and we find that $\sum_{\nu} \mid g_m^{\nu}(\mathbf{k}_{||},z_h) \mid^2$ is a smooth function of $\mathbf{k}_{||}$, even though $g_m^{\nu}(\mathbf{k}_{||},z_h)$ varies quickly with $\mathbf{k}_{||}$. The error introduced by such an approximation is estimated to be about 5%. This two-band model allows us to ignore Fano resonances[29] of high-lying excitons with the continuum levels of lower-lying excitons.

The bare exciton potential-energy function in our two-band model depends only on the magnitude of the wave-vector difference $q_{||} = \mid \mathbf{k}_{||} - \mathbf{k}'_{||} \mid$ and the free-electron and hole zone-center envelope functions. In Fig. 4 we have plotted the bare exciton potential $\bar{V}(q_{||})$ multiplied by $q_{||}$ as a function of $q_{||}$ for the HH1-CB1 and LH1-CB1 excitons.

These potential functions in Fig. 3 are well approximated by the simple expression[30]

$$q_{||} \bar{V}(q_{||}) = -(e^2/\epsilon_0)(1+\rho_0 q_{||})^{-1} , \quad (9)$$

where ρ_0 is a fitting parameter. The strict two-dimensional limit is obtained by letting $\rho_0 \to 0$. The potential in coordinate space, obtained by taking the Fourier-Bessel transform, is $\bar{V}(\rho) = -Z(\rho/\rho_0)e^2/\epsilon_0\rho$ with

$$Z(\rho/\rho_0) = (\pi/2)(\rho/\rho_0)[H_0(\rho/\rho_0) - N_0(\rho/\rho_0)] , \quad (10)$$

where $H_0(x)$ and $N_0(x)$ are the Struve and Neuman functions, respectively.[31] The fact that $q_{||} V(q_{||})$ can be ap-

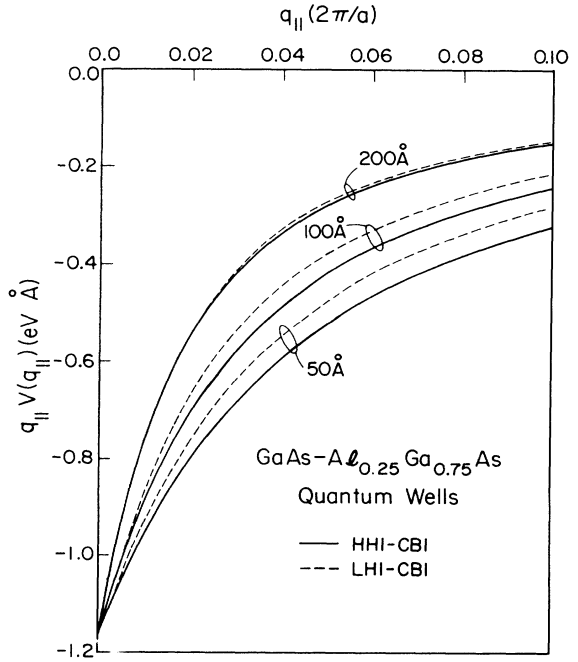

FIG. 3. Exciton potential energy function $q_{||}V(q_{||})$ in GaAs-$Al_{0.25}Ga_{0.75}As$ quantum wells for several well widths for HH1-CB1 excitons and LH1-CB1 excitons.

proximated by a simple analytic expression (9) not only simplifies the calculation of the exciton binding energy, but also makes feasible the calculation of the effect of final-state interaction on the absorption spectrum in the continuum regime, which we shall discuss in Sec. IV.

The variation in the exciton potential parameter ρ_0 with well width for several prominent excitons, which completely characterizes the bare Coulomb potential, is shown in Fig. 4 for GaAs-$Al_xGa_{1-x}As$ quantum wells having aluminum concentrations $x=0.25$. As seen in the figure there is a tendency for ρ_0 to decrease with decreasing well size as the exciton potential becomes increasingly two dimensional. At a critical well size the free-carrier wave functions start to leak into the surrounding $Al_xGa_{1-x}As$ barriers and the potential parameter starts to increase again.

To obtain the exciton Coulomb potential in the case for screening by free carriers, we must determine the form of the wave-vector-dependent dielectric function $\epsilon(q_{||})$ mentioned above. Within the random-phase approximation (RPA) the dielectric function $\epsilon(q_{||})$ is given by[32]

$$\epsilon(q_{||})=1+(q_s/q_{||})f_s(q_{||}) \times\{1-\Theta(q_{||}-2k_F)[1-(2k_F/q_{||})^2]^{1/2}\} , \quad (11)$$

where $q_s\equiv 2e^2m_d^*/\hbar^2\epsilon_0$ and k_F is the Fermi wave vector. m_d^* is the density-of-states effective mass for the free carrier. $f_s(q_{||})$ is the screening form factor[33] defined as

$$\int dz \int dz' \,|f_1(z)|^2\,|f_1(z')|^2 e^{-q_{||}|z-z'|} ,$$

where $f_1(z)$ is the first conduction- (for n-type doping) or valence- (for p-type doping) subband envelope function. This form factor is again fitted by the simple expression $(1+\bar{\rho}_0 q_{||})^{-1}$. For the n-type case, $\bar{\rho}_0$ is almost identical to ρ_0 for the LH1-CB1 excitation, because the conduction band and light-hole band have similar effective masses in the z direction. For the p-type case, $\bar{\rho}_0$ is about 10% smaller than ρ_0 for the HH1-CB1 exciton due to the difference in conduction-band and heavy-hole-band effective masses. For n-type quantum wells the density-of-states electron mass appearing in Stern's expression for $\epsilon(q_{||})$ is just $m_e^*=0.067m_0$, and for p-type quantum wells the density-of-states hole mass is taken to be $0.14m_0$

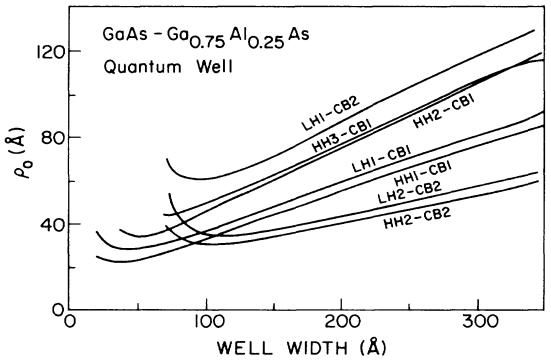

FIG. 4. Exciton potential parameter (ρ_0) versus well width (W) for GaAs-$Al_xGa_{1-x}As$ quantum wells with $x=0.25$ and 0.4.

characteristic of the filled HH1 subband.

The sharp discontinuity in the exciton Coulomb potential at $q_{||}=q_s$ makes the numerical evaluation of the exciton matrix elements difficult. We overcome this difficulty by fitting the wave-vector-dependent potential by an expression[34] of the form

$$\bar{V}(q_{||})/\epsilon(q_{||})=\frac{-e^2}{\epsilon_0 q_{||}}[(1+\rho_0 q_{||})^{-1}-e^{-bq_{||}}-Aq_{||}e^{-\alpha q_{||}^2}] , \quad (12)$$

where A, b, and α are adjustable parameters determined by a least-squares fit for any given values of $\bar{\rho}_0$, ρ_0, and k_F/q_s.

We solve for the exciton wave function variationally by expanding G_{nm} as a sum of Gaussians with exponents chosen to cover a broad physical range. The exciton binding energies and envelope wave functions are then obtained by solving a generalized eigenvalue problem for the expansion coefficients. All of the matrix elements are evaluated numerically, and, in particular, we use the computed nonparabolic band structures in the evaluation of the kinetic-energy matrix. The energy bands are nearly isotropic in the region of interest near the band edges, and with this approximation all the numerical integrals are one dimensional. Details of the calculation of the matrix elements are presented in Appendix B.

For quantum wells whose widths lie in the range from 60 to 300 Å, the most pronounced exciton absorption peaks in undoped quantum wells are the ground-state HH1-CB1, LH1-CB1, HH3-CB1, HH2-CB2, and LH1-CB2 excitons.[25,26,33–35] Binding energies of these excitons in undoped wells as functions of well width have previously been reported by us.[35] Those excitons associated with hole bands having negative-zone-center effective masses, i.e., LH1-CB1 and LH1-CB2 are seen to have significantly enhanced binding energies relative to other excitons. This is because the effect of a large joint density of states is to lower kinetic energy for the exciton.

The effects on exciton binding energy of p-type doping in GaAs-$Al_{0.25}Ga_{0.75}As$ quantum wells having widths of 100 and 200 Å is shown in Fig. 5, where we plot exciton binding energy as a function of the two-dimensional hole concentration. Referring to the figure, two things can be noted. First, all the exciton binding energies are seen to approach zero asymptotically for all except the HH1-CB1 excitons. The asymptotic behavior is consistent with the fact that in two dimensions an arbitrarily weak potential has at least one bound state. The HH1-CB1 exciton is seen to become an unbound resonance state at finite hole concentration, because the exciton envelope function $G_{11}(\mathbf{k}_{||})$ is restricted to regions of wave-vector space outside the Fermi sphere due to the partial filling of the HH1 subband. Hence, the resonance state is created by the resulting increase in the exciton's kinetic energy. Secondly, the binding energies of excitons associated with the "negative-mass" hole subbands (LH1 and HH3) approach zero much more slowly than those associated with other hole subbands.

For n-type doping those excitons involving CB1 become unbound resonance states at a large doping level.

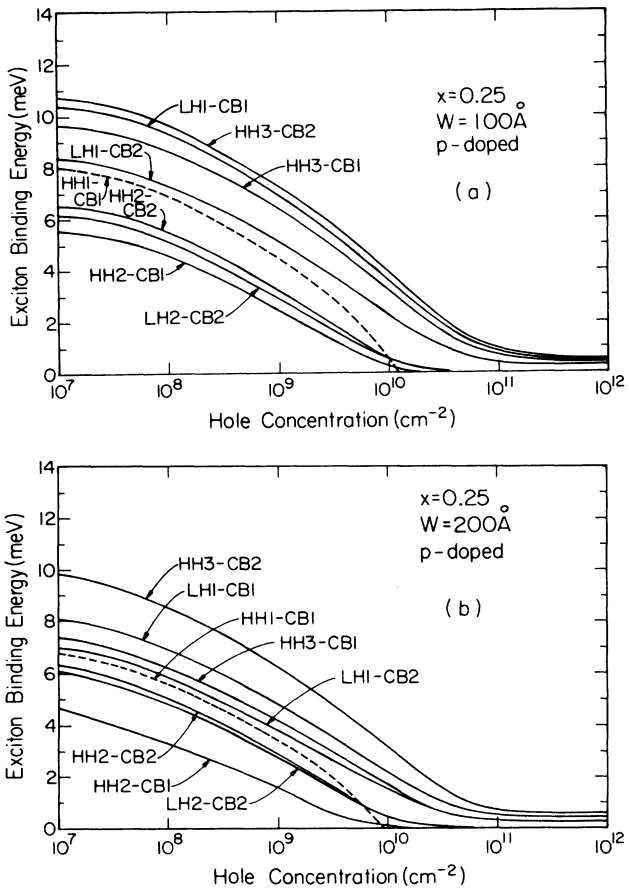

FIG. 5. Exciton binding energy versus hole concentration for (a) 100- and (b) 200-Å p-type modulation-doped GaAs-$Al_{0.25}Ga_{0.75}As$ quantum wells.

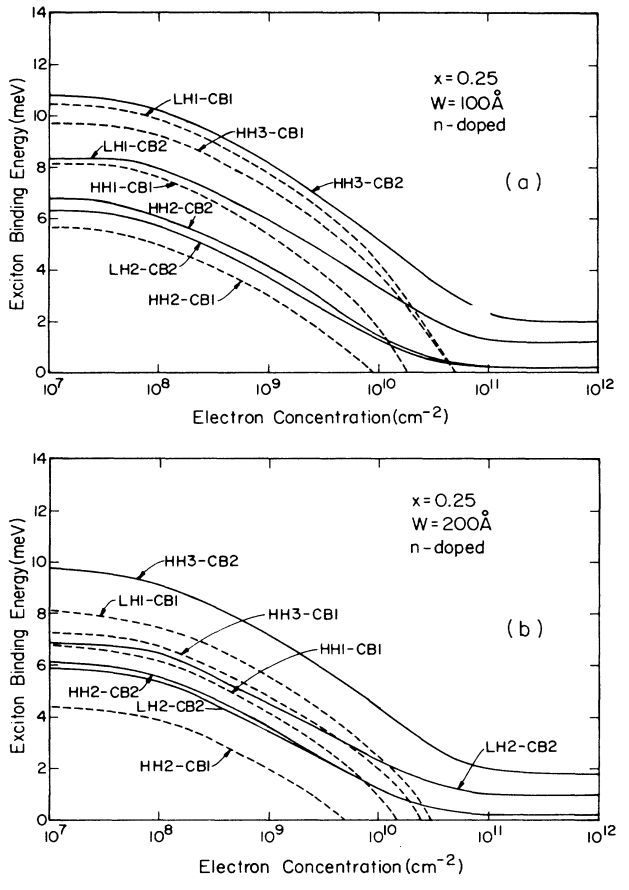

FIG. 6. Exciton binding energy versus electron concentration for (a) 100- and (b) 200-Å n-type modulation-doped GaAs-$Al_{0.25}Ga_{0.75}As$ quantum wells.

The binding energies in n-doped GaAs-$Al_{0.25}Ga_{0.75}As$ quantum wells as functions of the two-dimensional electron concentration are shown in Fig. 6 for 100- and 200-Å-wide wells. Here the LH1-CB2, HH2-CB2, and LH2-CB2 exciton binding energies approach zero asymptotically and all other excitons become unbound resonances at some finite doping level.

IV. OPTICAL PROPERTIES OF MODULATION-DOPED QUANTUM WELLS

In this section we calculate the optical properties of GaAs-$Al_xGa_{1-x}As$ quantum-well structures including the excitonic effect. In particular we are able to calculate the absorption spectrum in absolute units and compare our results with available data. We consider absorption for the usual experimental situation where unpolarized light is incident along the growth direction (i.e., x,y polarization), and for linearly polarized light with the electric field vector oriented along the growth direction z and Poynting vector directed along x (i.e., z polarization). The latter case is of interest because transitions involving heavy-hole components are forbidden as shown below.

The band-to-band absorption, neglecting final-state Coulomb interaction, is obtained by applying Fermi's golden rule. The total band-to-band absorption coefficient $\alpha_B(\hbar\omega)$ is given by summing over each of the individual subband-to-subband transitions. Thus

$$\alpha_B(\hbar\omega)=\sum_{n,m}\alpha_{n,m}(\hbar\omega)$$

where $\alpha_{n,m}(\hbar\omega)$, the band-to-band transition from valence subband m to conduction subband n, is given by[36]

$$\alpha_{n,m}(\hbar\omega)=\frac{4\pi^2e^2\hbar}{n_0cm_0^2V}\left[\frac{1}{\hbar\omega}\right]\times\sum_{\mathbf{k}_{||}}|\hat{\epsilon}\cdot\mathbf{P}_{nm}(\mathbf{k}_{||})|^2\times\delta(E_m^h(\mathbf{k}_{||})-E_n^e(\mathbf{k}_{||})+\hbar\omega)\,. \quad (13)$$

Here it is understood that in the case of band filling due to modulation doping, the summation over $\mathbf{k}_{||}$ is restricted to regions in $\mathbf{k}_{||}$ space outside the Fermi sphere. $E_m^h(\mathbf{k}_{||})$ and $E_n^e(\mathbf{k}_{||})$ are the valence and conduction subbands, m_0 is the free-electron mass, n_0 is the refractive index, $\hat{\epsilon}$ is the polarization vector, and $\hbar\omega$ is the energy of the incident photons. Throughout this paper, we take the index of refraction n_0 of all GaAs-$Al_xGa_{1-x}As$ quantum wells to be a constant ($n_0=3.4$). It has been shown[37,38] that the

variation of n_0 in the energy range of interest is at most 5%. In (13), the optical matrix element $P_{nm}(\mathbf{k}_{||})$ is given by $\mathbf{P}_{nm}(\mathbf{k}_{||})=\langle\psi_m^h|\mathbf{P}|\psi_n^e\rangle$. Here ψ_m^h and ψ_n^e are the valence- and conduction-subband wave functions at $\mathbf{k}_{||}$. In the envelope-function approximation, the optical matrix element is given by

$$\hat{\epsilon}\cdot\mathbf{P}_{nm}(\mathbf{k}_{||})=\sum_{\nu,\sigma}\langle g_m^\nu|f_n^\sigma\rangle\langle\psi_\nu^h|\hat{\epsilon}\cdot\mathbf{P}|\psi_\sigma^e\rangle\ . \tag{14}$$

The hole spin $\nu=-\frac{3}{2},\ -\frac{1}{2},\ \frac{1}{2},\ \frac{3}{2}$ and the electron spin $\sigma=-\frac{1}{2},\ \frac{1}{2}$. The envelope functions g_m^ν and f_n^σ and the bulk Bloch functions ψ_ν^h and ψ_σ^e were defined earlier. The nonvanishing matrix elements $\langle\psi_\nu^h|\hat{\epsilon}\cdot\mathbf{P}|\psi_\sigma^e\rangle$ involving bulk Bloch states are easily derived. The electron Bloch states are given by $|\psi_{1/2}^e\rangle=|s\rangle\alpha$ and $|\psi_{-1/2}^e\rangle=|s\rangle\beta$, where α and β denote the up and down electron spinors and $|s\rangle$ is the s-like conduction-band Bloch state. For the holes, the Bloch states are linear combinations of the products of electron spinor and the p-like valence-band Bloch states $|x\rangle$, $|y\rangle$, and $|z\rangle$. They are given by

$$|\psi_{3/2}^h\rangle=\frac{-1}{\sqrt{2}}(|x\rangle+i|y\rangle)\alpha\ ,$$

$$|\psi_{1/2}^h\rangle=\frac{-1}{\sqrt{6}}[(|x\rangle+i|y\rangle)\beta-2|z\rangle\alpha]\ ,$$

$$|\psi_{-1/2}^h\rangle=\frac{1}{\sqrt{6}}[(|x\rangle-i|y\rangle)\alpha+2|z\rangle\beta]\ ,$$

and

$$|\psi_{-3/2}^h\rangle=\frac{1}{\sqrt{2}}(|x\rangle-i|y\rangle)\beta\ .$$

The evaluation of the matrix elements is straightforward and the nonvanishing matrix elements are given by

$$i\langle\psi_{\pm3/2}^h|p_y|\psi_{\pm1/2}^e\rangle=\langle\psi_{\pm3/2}^h|p_x|\psi_{\pm1/2}^e\rangle=\mp\frac{1}{\sqrt{2}}\langle x|p_x|s\rangle\ ,$$

$$i\langle\psi_{\pm1/2}^h|p_y|\psi_{\mp1/2}^e\rangle=\langle\psi_{\pm1/2}^h|p_x|\psi_{\mp1/2}^e\rangle=\mp\frac{1}{\sqrt{6}}\langle x|p_x|s\rangle\ ,$$

and

$$\langle\psi_{\pm1/2}^h|p_z|\psi_{\pm1/2}^e\rangle=\frac{2}{\sqrt{6}}\langle x|p_x|s\rangle\ .$$

Here we make use of the orthonormality of the spin states α and β and the fact that under the symmetry properties of the group O_h, $\langle x|p_x|s\rangle=\langle y|p_y|s\rangle=\langle z|p_z|s\rangle$ while all other such matrix elements vanish. The squared matrix element $(1/2m_0)|\langle x|p_x|s\rangle|^2$ for GaAs which appears in our calculation is taken to be 25.7 eV as given in Ref. 11.

In bulk semiconductors the optical matrix element is a slowly varying function of $\mathbf{k}$ and may safely be approximated by its value at $\mathbf{k}=0$. This approximation has also been made by a number of authors in the study of superlattices and quantum wells.[18] The widely known $\Delta n=0$ selection rule for transitions between subbands is based on the observation that in the envelope-function approximation $\mathbf{P}_{nm}(\mathbf{k}_{||}=0)$ vanishes unless $n=m$. Furthermore, the absorption coefficient in this approximation is given by (apart from a constant factor)

$$\alpha(\hbar\omega)\sim\frac{2}{\hbar\omega m_0}\sum_{n,m}|\hat{\epsilon}\cdot\mathbf{P}_{nm}(0)|\,\delta_{n,m}J_{n,m}(\hbar\omega)\ , \tag{15}$$

where $J_{nm}(\hbar\omega)$ is the joint density of states between valence subband m and conduction subband n. For two-dimensional parabolic subbands $J_{nm}(\hbar\omega)$ is a step function. It has been pointed out recently,[25,26] however, that for superlattices and quantum wells the approximation $\mathbf{P}_{nm}(\mathbf{k}_{||})\simeq\mathbf{P}_{nm}(0)$ is a very poor one. We find that $\mathbf{P}_{nm}(\mathbf{k}_{||})$ is rapidly varying even for small values of $\mathbf{k}_{||}$ due to the strong mixing of heavy- and light-hole states by the off-diagonal elements in the valence-band Hamiltonian $H_{\nu\nu'}$. Thus it is necessary to retain the $\mathbf{k}_{||}$ dependence of $\mathbf{P}_{nm}(\mathbf{k}_{||})$ in our analysis. Fortunately, we have found that the squared optical matrix elements $|\hat{\epsilon}\cdot\mathbf{P}_{nm}(\mathbf{k}_{||})|^2$ and the energy bands $E_m^h(\mathbf{k}_{||})$ and $E_n^e(\mathbf{k}_{||})$ are nearly independent of the direction of $\mathbf{k}_{||}$, allowing us to make an isotropic approximation. The integration over $\mathbf{k}_{||}$ in the formula for the absorption coefficient is one dimensional in the isotropic approximation.

To include the effects of the final-state Coulomb interaction, the individual band-to-band absorption coefficients $\alpha_{n,m}(\hbar\omega)$ must be multiplied by a Coulomb enhancement factor which is proportional to the probability of finding the electron and hole at the same position. To calculate the enhancement factor, we must solve the exciton effective-mass equation (7) in the continuum regime for each pair of conduction and valence subbands. For simplicity, we approximate the energy dispersion for the exciton relative motion $[E_n^e(\mathbf{k}_{||})-E_m^h(\mathbf{k}_{||})]$ by an effective-mass expression, $\hbar^2k_{||}^2/2\mu_{nm}$, where μ_{nm} denotes the reduced effective mass for the exciton constructed by the nth conduction subband and the mth valence subband. μ_{nm} is chosen so that the exciton binding energy obtained in this approximation is identical to that obtained by solving (7). Transforming (7) into the real space yields

$$\left[-\frac{\hbar^2\nabla_\rho^2}{2\mu_{nm}}-V_{nm}(\rho)\right]G_{nm}(\rho)=EG_{nm}(\rho)\ , \tag{16}$$

where $V_{nm}(\rho)$ is the Fourier-Bessel transform of $V_{nm}(q_{||})$. Using the approximations given by (9) and (12), we find that $V_{nm}(\rho)$ takes the simple analytic form

$$V(\rho)=-Z(\rho/\rho_0)e^2/\epsilon_0\rho\quad\text{(for the undoped case)}$$

and

$$V(\rho)=-\frac{e^2}{\epsilon_0\rho}\left[Z(\rho/\rho_0)-\frac{\rho}{(\rho^2+b^2)^{1/2}}-\left[\frac{A\rho}{2\alpha}\right]e^{-\rho^2/4\alpha}\right]\quad\text{(for the doped case)}\ , \tag{17}$$

where $Z(\rho/\rho_0)$ is given by (10), and the fitting parameters b, A, and α depend on $\bar{\rho}_0$, ρ_0 and k_F/q_s.

Since $V(\rho)$ is analytic, (16) can be solved by simple integration and the Coulomb enhancement factor is given by $h(E)=|G_E(0)/\bar{G}_E(0)|^2$, where $G_E(0)$ is the solution to (16) at $\rho=0$ with energy E and $\bar{G}_E(0)$ is the corresponding solution for the case $V(\rho)=0$ (i.e., free-particle solution). The result for the Coulomb enhancement factor for the undoped case is shown in Fig. 7. Here the exciton reduced mass is taken to be $\mu=0.045\mu_0$, a typical value for most excitons in GaAs quantum wells. When $\rho_0=0$, the exciton potential reduces to $-\epsilon^2/\epsilon_0\rho$ (the pure two-dimensional limit) and the result shown in Fig. 7 is in agreement with the exact analytic solution[39]

$$h(E)=2/\{1+\exp[-\pi/(E/E_0)^{1/2}]\}\ , \tag{18}$$

where E_0 is the binding energy of the two-dimensional exciton. When $\rho_0\rightarrow\infty$, the Coulomb enhancement factor reduces to 1 as expected. For most quantum wells of interest ($W=50$–300 Å), ρ_0 is between 20–100 Å and we find that the enhancement factor is between 1.5 and 1.3 at $E=0$ (the threshold) and gradually decreases to 1 at $E\rightarrow\infty$.

The effect of carrier screening on the Coulomb enhancement factor is illustrated in Fig. 8 for $\rho_0=34$ Å, which is appropriate for the $\Delta n=0$ excitons for GaAs-$Al_{0.75}Ga_{0.25}As$ quantum wells with $W\sim 100$ Å. Here, the two-dimensional carrier density (n) is related to the Fermi wave vector k_F by the expression, $n=k_F^2/2\pi$. For k_F between 0.005 to 0.05 $Å^{-1}$ (i.e., n between 4×10^{10} cm^{-2} and 4×10^{12} cm^{-2}), we find that the enhancement factor is sharply peaked near the threshold, indicating a "resonance." For $k_F>0.1$ $Å^{-1}$ ($n>1.6\times10^{13}$ cm^{-2}), the resonance disappears and the enhancement factor approaches 1 as k_F increases further.

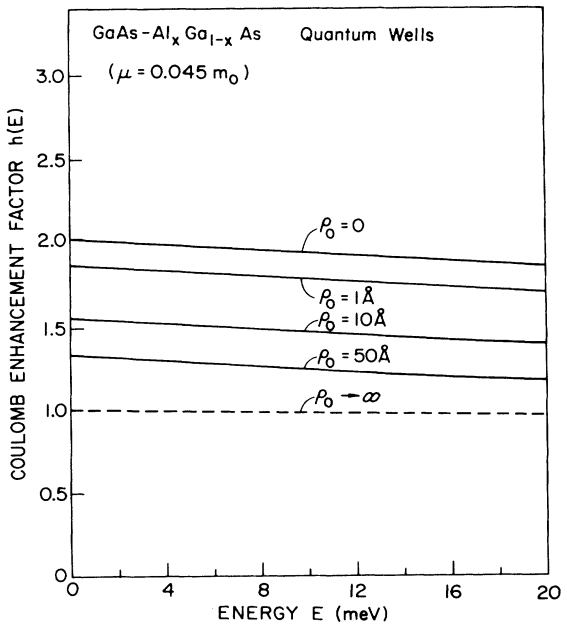

FIG. 7. Coulomb enhancement factor for undoped GaAs-$Al_xGa_{1-x}As$ quantum wells for various values of exciton potential parameters (ρ_0).

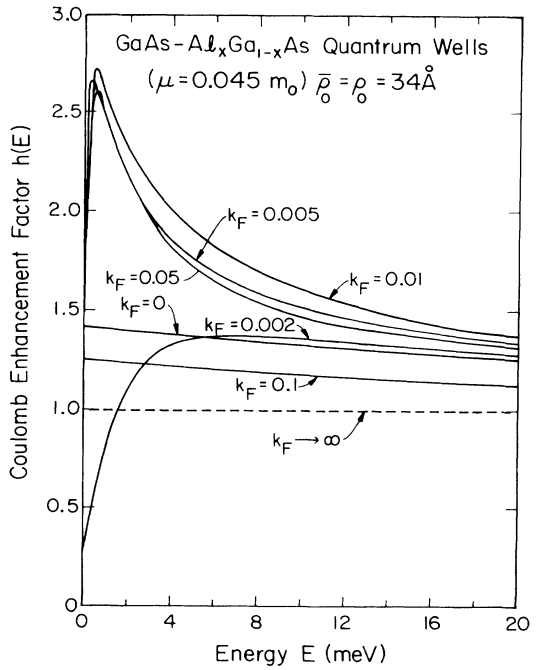

FIG. 8. Coulomb enhancement factor for modulation-doped GaAs-$Al_xGa_{1-x}As$ quantum wells for various values of Fermi wave vectors k_F (in units of $Å^{-1}$).

In Fig. 9 we have plotted the component absorption spectra $\alpha_{m,n}(\hbar\omega)$, including the Coulomb enhancement effect, for subband-to-subband transitions involving the first six valence subbands and the first two conduction subbands for an undoped 102-Å GaAs-$Al_{0.27}Ga_{0.73}As$ quantum well for incident photons having (x,y) polarization. In the figures absorption spectra for transitions to CB1 are solid curves and corresponding spectra for transitions to CB2 are dashed curves. The individual curves are labeled by the valence-subband index m. The subband-to-subband transitions are quite complicated and the rapidly varying nature of the individual subband absorption curves reflects valence-band mixing. The total band-to-band absorption spectra for (x,y) and z polarizations are shown in Figs. 10 and 11 (dashed curves). It is found that the overall shape of the total absorption obtained by adding up the individual subband-to-subband absorption curves is close to the staircase function predicted by the simple-model calculation (15), although each step tends to decline faster than $1/\omega$ at higher energy due to the decrease of optical matrix element with increasing $\mathbf{k}_{||}$. Thus, despite the strong variations of the optical matrix element for various component transitions, the net band-to-band absorption is nearly featureless. This is not surprising, since the sum of oscillator strengths for optical transitions from two interacting valence states to a given conductor band must remain constant despite the mixing. The peak structure seen in Fig. 10 for the B(LH1-CB1) transition is due to the negative zone center effective mass of the LH1 subband. The electronlike curvature of the LH1 subband gives the LH1-CB1 transition an exception-

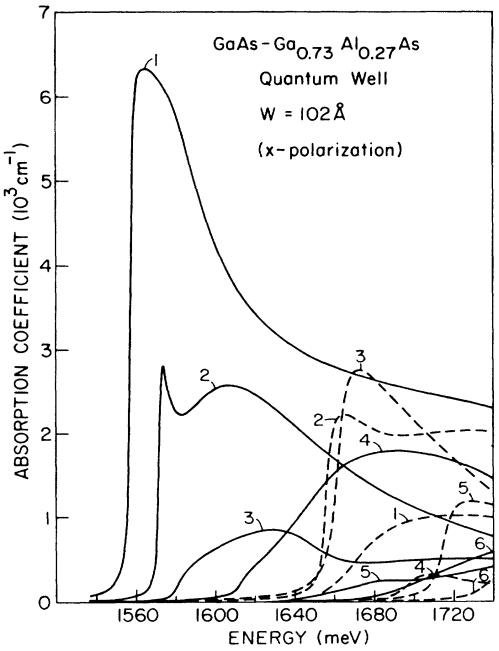

FIG. 9. Subband-to-subband absorption coefficient for transitions from the first six valence subbands (labeled 1—6) to the first (solid curves) and second (dashed curves) conduction subbands for a 100-Å GaAs-$Al_{0.27}Ga_{0.73}As$ quantum well for (x,y) polarization.

ally large joint density of states at the band edge, hence the sharp peak near 1580 meV. To include the effects of absorption due to the bound states of free excitons, we make use of the exciton envelope wave functions $G_{nm}(\mathbf{k}_{||})$ and binding energies and the band-to-band optical matrix elements $P_{nm}(\mathbf{k}_{||})$ described earlier. The exciton oscillator

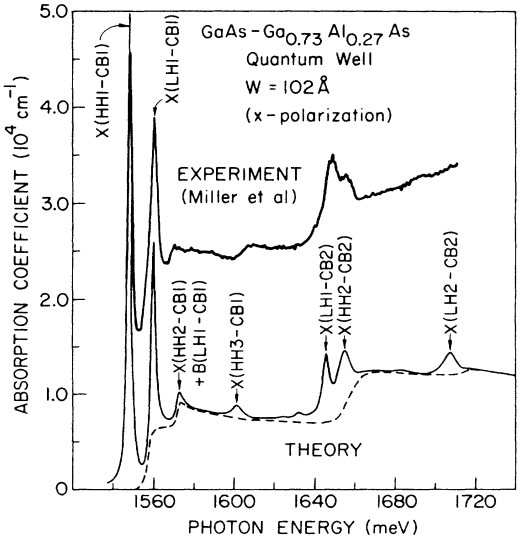

FIG. 10. Absorption coefficient of a 102-Å GaAs-$Al_{0.27}Ga_{0.73}As$ quantum well for incident photons with x,y polarization; solid curve: with excitons; dashed curve: without excitons. Also included for comparison is the photoexcitation spectra of Miller *et al.* (Ref. 40).

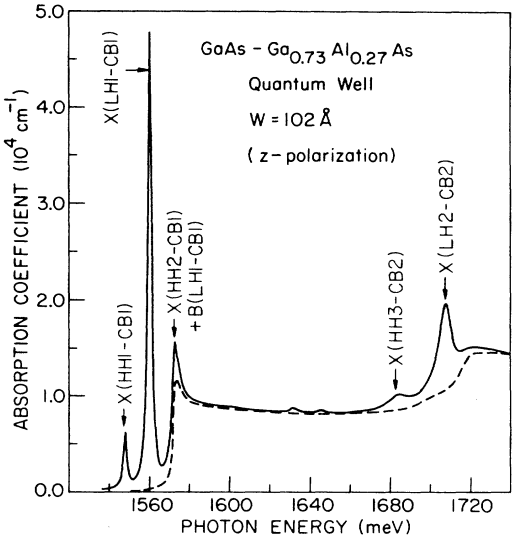

FIG. 11. Absorption coefficient of a 102-Å GaAs-$Al_{0.27}Ga_{0.73}As$ quantum well for incident photons with z polarization; solid curve: with excitons; dashed curve: without excitons.

strength per unit area is given by

$$f_{nm}=\frac{2}{\hbar\omega m_0}\left|\sum_{\mathbf{k}_{||}} G_{nm}(\mathbf{k}_{||})\hat{\epsilon}\cdot\mathbf{P}_{nm}(\mathbf{k}_{||})\right|^2 . \tag{19}$$

Here, again the summation over $\mathbf{k}_{||}$ is restricted to the regions in $\mathbf{k}_{||}$ space outside the Fermi sphere in the case of modulation doping.

The absorption coefficient including the excitonic effect is given by

$$\alpha(\hbar\omega)=\sum_{nm}\left[\frac{4\pi^2e^2\hbar}{n_0cm_0V}f_{nm}\Delta_{nm}(\hbar\omega-E_{nm}^{\rm ex})+\tilde{\alpha}_{nm}(\hbar\omega)\right] , \tag{20}$$

where $\Delta_{nm}(E)\equiv(\Gamma_{nm}/\pi)(E^2+\Gamma_{nm}^2)^{-1}$ is a Lorentzian function of half with Γ_{nm} which describes the effects of line broadening for the nm transition. $E_{nm}^{\rm ex}$ is the ground-state energy of the nm exciton,

$$\tilde{\alpha}_{nm}(E)\equiv\int\alpha_{nm}(E')h_{nm}(E')\Delta(E-E')dE' ,$$

where $h_{nm}(\hbar\omega)$ is the Coulomb enhancement factor for the nm band-to-band transition, and $\alpha_{nm}(\hbar\omega)$ is the band-to-band absorption given by (13). For Γ_{nm}, we use the empirical rule $\Gamma_{nm}=\Gamma_0 nn'$, where n and n' are the principal quantum numbers for the electron and the heavy- or light-hole quantum-well states. Γ_0 is an empirical parameter which can be adjusted to fit the empirical data.

The theoretically predicted absorption spectra for an undoped 102-Å GaAs-$Al_{0.27}Ga_{0.73}As$ quantum well for x,y and z polarizations are shown in Figs. 10 and 11 (solid curves). The photoexcitation spectrum measured by Miller *et al.* is also shown in Fig. 10 for comparison. Note that the absolute units for the experimental data are unknown here. The parameter Γ_0 used in the theoretical spectra is 1 meV. Fairly good agreement between the

theory and experiment is obtained. There is discrepancy in the energy positions of the theoretical X(HH3-CB1) peak and the corresponding experimental peak structure. This is probably due to the uncertainty in the heavy-hole effective mass used in the theoretical model. Miller has shown that the peak position matches well with the X(HH3-CB1) transition if one uses $m_{HH}=0.34m_0$.[35]

We can also compare the theoretical absorption spectra with the experimentally measured spectra directly (both in absolute units). This is shown in Fig. 12 for 116- and 210-Å GaAs-$Al_{03}Ga_{0.7}As$ quantum wells. The data was taken by Masselink *et al.*[41] The broadening parameter Γ_0 in the theoretical spectra is taken to be 1 meV. The absolute magnitude of the theoretical spectrum for the transitions to the first conduction subband agrees well with the data. For transitions to higher conduction subbands, the theoretical prediction is somewhat lower. For higher-energy transitions, the theoretical model is less justified in that the nonparabolity of the conduction band which is not included in our model becomes more important and the leaking of the electron wave function into the $Al_xGa_{1-x}As$ region becomes more serious. It should be noted that the experimental data was taken for a superlattice with a 100-Å-wide $Al_{0.3}Ga_{0.7}As$ barrier, instead of a single quantum well. The interaction of electron wave functions in adjacent wells will affect the absorption. This effect is also larger for higher-energy transitions. The measured absorption spectra does not have resolution as good as the photoexcitation spectra, so the X(LH1-CB2) and X(HH2-CB2) transitions remain unresolved.

We have studied the oscillator strengths of prominent excitons systematically as functions of quantum-well width. The theoretical results for undoped GaAs-$Al_{0.25}Ga_{0.75}As$ quantum wells for the (x,y) polarization have been previously reported.[35] The corresponding results for the z polarization are shown in Fig. 13. The exciton oscillator strengths are found to be complicated functions of well width. In general, there is a trend toward decreasing oscillator strength with increasing well width for moderately wide wells on account of wave-function spreading. Note that in the absence of band hybridization, the $\Delta n=0$ exciton oscillator strengths are proportional to $|G(0)|^2$.

For wide wells, the oscillator strength per unit area falls off approximately as $1/W$ where W is the well width. This dependence can be seen as follows. Since f_{nm} is proportional to $|G(0)|^2$, then in a quantum well $f_{nm}\sim a^{-2}$ where a is the extent of the exciton in the x,y plane. For moderately wide wells $a\sim W^{1/2}$ and $f_{nm}\sim 1/W$.[41] For very narrow wells, this trend is reversed as the exciton wave function spills out of the well into the $Al_xGa_{1-x}As$ barrier and thus the oscillator strength typically has a maximum at some critical width. This picture is complicated by hybridization of the hole wave functions. In addition to the $\Delta n=0$ excitons there are $\Delta n\neq 0$ forbidden excitons which share oscillator strength with the $\Delta n=0$

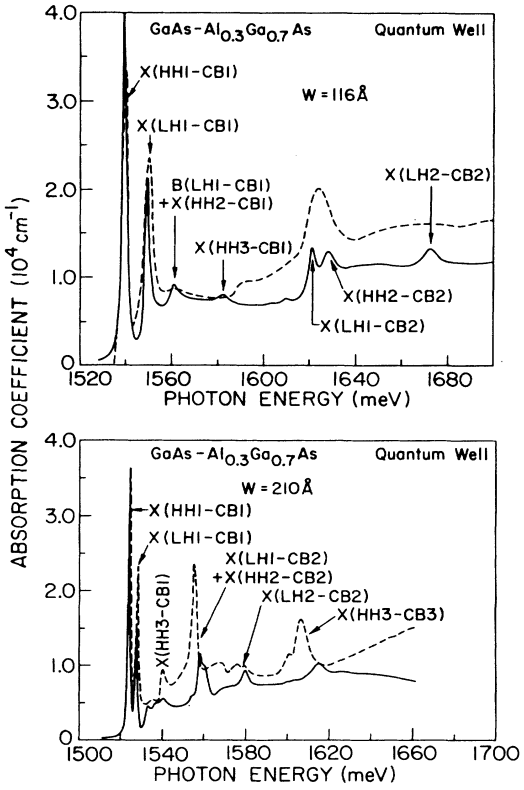

FIG. 12. Absorption spectra of 116- and 210-Å GaAs-$Al_{0.3}Ga_{0.7}As$ quantum wells; solid curves: theory; dashed curves: experimental data taken from Ref. 43.

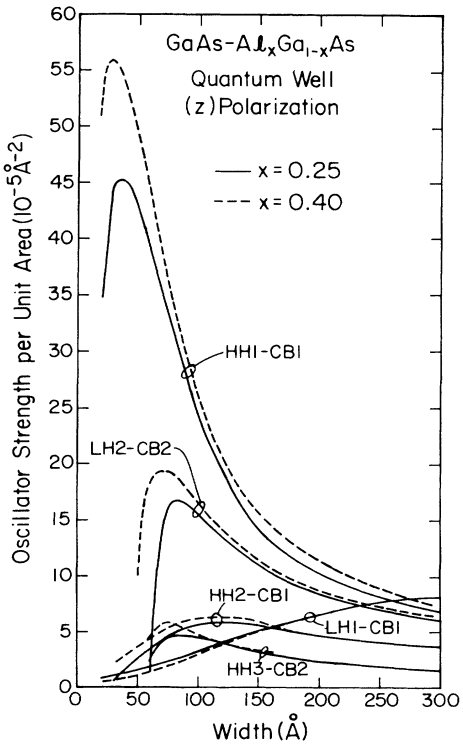

FIG. 13. Exciton oscillator strengths per unit area for several prominent excitons versus well width in undoped GaAs-$Al_{0.25}Ga_{0.75}As$ quantum wells for z polarization.

excitons through mixing of their valence-subband wave functions. Thus the LH1-CB2 exciton corresponding to a parity forbidden $\Delta n = 1$ transition acquires a giant oscillator strength at the expense of the HH2-CB2 exciton since the LH1 and HH2 states are nearly degenerate in energy and strongly mixed. In this situation the LH1-CB2 and HH2-CB2 exciton peaks form a closely spaced pair with HH2-CB2 being the stronger of the two transitions.

The absorption spectra of p-type modulation-doped spectra of GaAs-$Al_xGa_{1-x}As$ quantum wells are shown in Figs. 14 and 15. In Fig. 14, $W = 115$ Å, $x = 0.44$, and the hole concentration (n_h) is 5.4×10^{10} cm^{-2}. In Fig. 15, $W = 90$ Å, $x = 0.45$, and hole concentration is about 10 times higher ($n_h = 5.3\times10^{11}$ cm^{-2}). To compare with the experimental data, the excitation spectra measured by Miller and Kleinman[8] are included in these figures. We find that in both cases ($n_h = 5.4\times10^{10}$ cm^{-2} and 5.3×10^{11} cm^{-2}), the HH1-CB1 exciton is unbound due to the blocking of HH1 states with energies below the Fermi level, and the other excitons are sufficiently screened so that they do not appear as distinct features. The structure seen in these figures are mostly due to the band-to-band transitions (dashed curves). The LH1-CB1 peak is mainly due to the sharp density of states near the threshold where the associated hole subband structure has a "negative" effective mass as previously discussed. A similar theoretical absorption spectrum for a 100-Å p-type doped GaAs-$Al_{0.4}Ga_{0.6}As$ quantum well was reported in a previous paper.[14] In that calculation, the carrier screening and finite-well effect on the Coulomb enhancement factor was neglected.[42] As demonstrated in Fig. 8, the carrier screening effect on the final-state interaction will give rise to a resonance structure in the Coulomb enhancement factor. This is most clearly seen in the sharp peaks labeled LH1-CB2 and HH2-CB2 in Figs. 14 and 15. These structures are in reasonable agreement with those of the excitation spectra.[8] The band-to-band transition calculated here was broadened by 1 meV, and the exciton peaks were broadened by $\Gamma_{nn'} = 2$ meV $\times n \times n'$ where n and n' are principal quantum numbers for the electron and hole states.

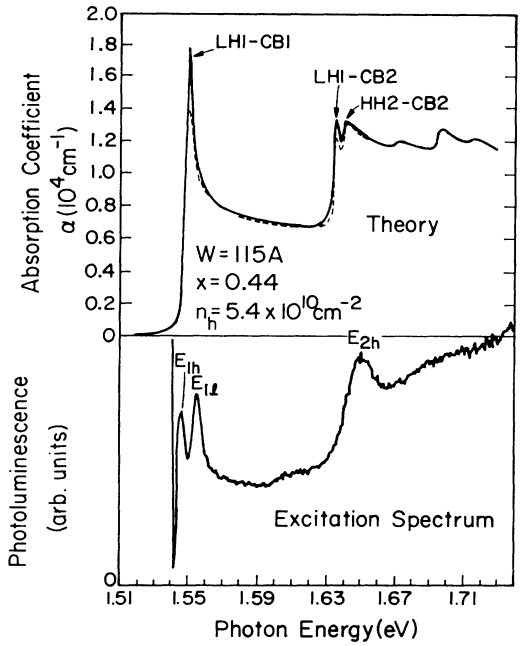

FIG. 14. Absorption spectrum of a 115-Å modulation-doped GaAs-$Al_{0.44}Ga_{0.56}As$ quantum well, with hole concentration $n_h = 5.4\times10^{10}$ cm^{-2}; solid curve: with excitons; dashed curve: without excitons. The excitation spectrum of Ref. 8 is included for comparison.

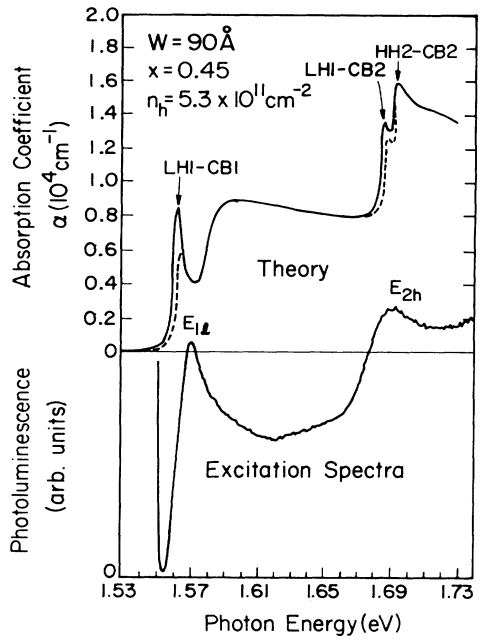

FIG. 15. Absorption spectrum of a 90-Å modulation-doped GaAs-$Al_{0.45}Ga_{0.55}As$ quantum well, with hole concentration $n_h = 5.3\times10^{11}$ cm^{-2}; solid curve: with excitons; dashed curve: without excitons. The excitation spectrum of Ref. 8 is included for comparison.

In Fig. 14, a peak labeled E_{1h} was observed in the excitation spectrum at 5 K. However, at lower temperatures this peak is suppressed.[8] This peak is most likely due to the HH1-CB1 transition. Although the HH1-CB1 exciton is unbound due to the blocking effect, a peak structure in absorption near the threshold for band-to-band transition is still possible if the many-body effect is appropriately included as in Ref. 27.

In Fig. 15, the theoretical absorption spectrum indicates a suppression of the HH1-CB1 band-to-band transition for energies below ~ 1.58 eV due to the Burstein-Moss blocking effect.[43] However, this feature is not observed in the corresponding excitation spectrum as shown in Fig. 18. At present, we have no satisfactory explanation for the discrepancy.

Figure 16 shows the comparison between the theoretical absorption spectrum and the experimental excitation spectrum for a 104-Å n-type modulation-doped GaAs-$Al_{0.3}Ga_{0.7}As$ quantum well with electron concentration $n_e = 1.4\times10^{11}$ cm^{-2}. For n-type doping, all excitons associated with CB1 are unbound at this concentra-

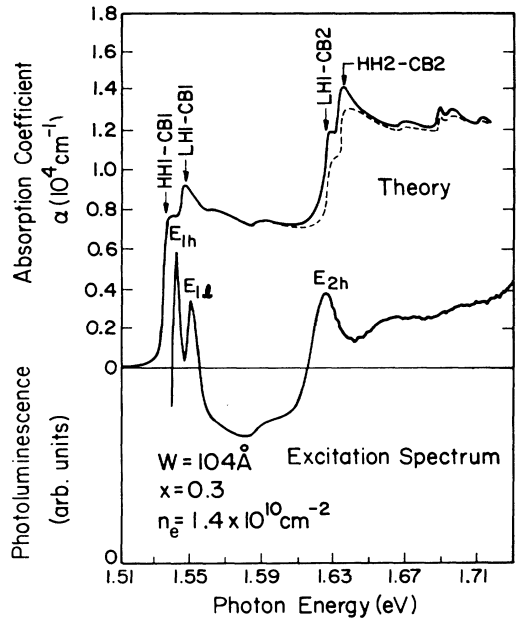

FIG. 16. Absorption spectrum of a 104-Å modulation-doped GaAs-$Al_{0.3}Ga_{0.7}As$ quantum well with electron concentration $n_e = 1.4 \times 10^{11}$ cm^{-2}; solid curve: with excitons; dashed curve: without excitons. The excitation spectrum of Ref. 8 is included for comparison.

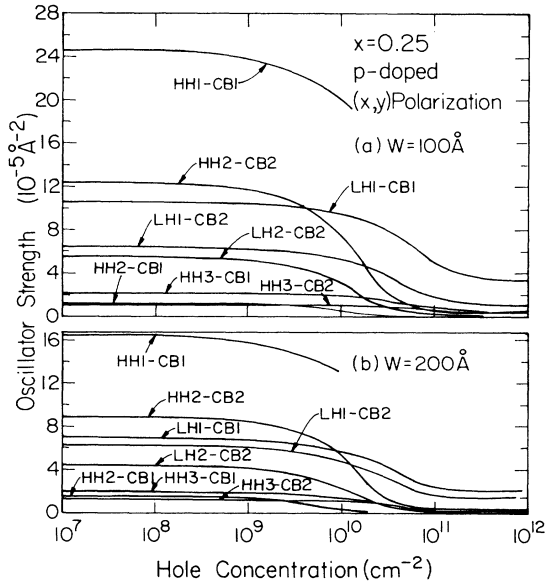

FIG. 17. Exciton oscillator strengths per unit area for several prominent excitons versus hole concentration in (a) 100- and (b) 200-Å modulation-doped GaAs-$Al_{0.25}Ga_{0.75}As$ quantum wells for x,y polarization.

tion, because of the blocking of CB1 states with energies below the Fermi level. Thus the theoretical spectrum shows no exciton contributions for photon energies below 1.59 eV. Some structures appear near 1.54 eV due to the Coulomb enhancement factor in the LH1-CB1 band-to-band transition. The excitation spectrum shows distinct peaks labeled E_{1h} and E_{1l}, which probably correspond to the Mahan excitons[27] and cannot be accounted for without including the many-body effect. The second peak labeled E_{2h} in the excitation spectrum, however, is accounted for by our present theoretical calculation. The broadening parameters used here are the same as in Figs. 14 and 15.

We have also performed systematic studies of the effects of p- and n-type modulation doping on exciton oscillator strengths in GaAs-$Al_xGa_{1-x}As$ quantum wells. The dependence of exciton oscillator strengths on carrier concentration in 100- and 200-Å p-type doped GaAs-$Al_{0.25}Ga_{0.75}As$ quantum wells are shown in Figs. 17 and 18. We find that the exciton oscillator strength decreases monotonically to zero as a function of the two-dimensional carrier concentration. Screening of the Coulomb interaction by the free-hole carriers results in a decrease in $|G(0)|^2$ as the exciton becomes more loosely bound and consequently more delocalized in the x-y plane. The oscillator strengths of those excitons associated with negative-mass hole subbands (LH1 and HH3) are seen to approach zero much more slowly than those excitons associated with other hole subbands. This results in a curious phenomenon, namely that for free-carrier concentrations above a certain critical value a forbidden exciton associated with a negative-mass hole subband can become stronger than the allowed exciton with which it shares oscillator strength if the allowed exciton is associated with a positive-mass hole subband. The best example of this can be seen in the closely spaced pair of excitons

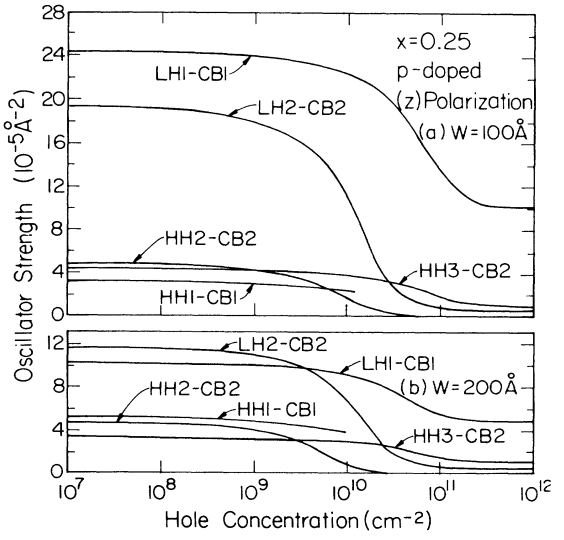

FIG. 18. Exciton oscillator strengths per unit area for several prominent excitons versus hole concentration in 100- and 200-Å modulation-doped GaAs-$Al_{0.25}Ga_{0.75}As$ quantum wells for z polarization.

LH2-CB2 and HH2-CB2 mentioned previously. Here the parity forbidden LH1-CB2 exciton associated with the negative-mass LH1 subband shares oscillator strength with the allowed HH2-CB2 exciton associated with positive-mass HH2 subband through strong mixing of LH1 and HH2. As the hole concentration increases the oscillator strength curves for LH1-CB2 and HH2-CB2 are seen to cross and LH1-CB2 then becomes the stronger transition of the two.

In Figs. 19 and 20 we plot the exciton oscillator strength per unit area as a function of electron concentration for 100- and 200-Å n-type doped GaAs-$Al_{0.25}Ga_{0.75}As$ quantum wells. The effect of electron screening is to dampen the oscillator strength as seen in the figure. As in the p-type doped case, the strength of the LH1-CB2 exciton declines less rapidly with doping level than the HH2-CB2 and LH2-CB2 excitons due to the negative effective mass of LH1.

V. SUMMARY AND CONCLUSION

In summary, we have carried out a systematic study of electronic and optical properties of modulation-doped GaAs-$Al_xGa_{1-x}As$ quantum wells. We consider cases in which the $Al_xGa_{1-x}As$ barriers are doped either n or p type and the GaAs wells are filled with a gas of free carriers. We find that the electronic valence-band structure is very complicated due to strong mixing of heavy and light holes. The valence subbands are highly nonparabolic and in particular some valence subbands have negative zone center effective masses. Zone center masses are studied and found to be sensitive to variations in well width but relatively insensitive to doping level. Exciton binding energies and oscillator strengths are found to be sensitive functions of both well width and doping level. Because of valence-band mixing all exciton transitions are dipole allowed. Excitons associated with negative zone center hole masses tend to have enhanced binding energies and oscillator strengths. Those excitons formed from filled subband states give rise to unbound resonance states at finite doping levels while those excitons formed from the unfilled subband states are weakly bound and have sharply reduced oscillator strengths due to screening by free carriers. The band-to-band absorption is found to be modified by screening effects. The screened final-state interaction gives rise to a sharp resonance peak in the Coulomb

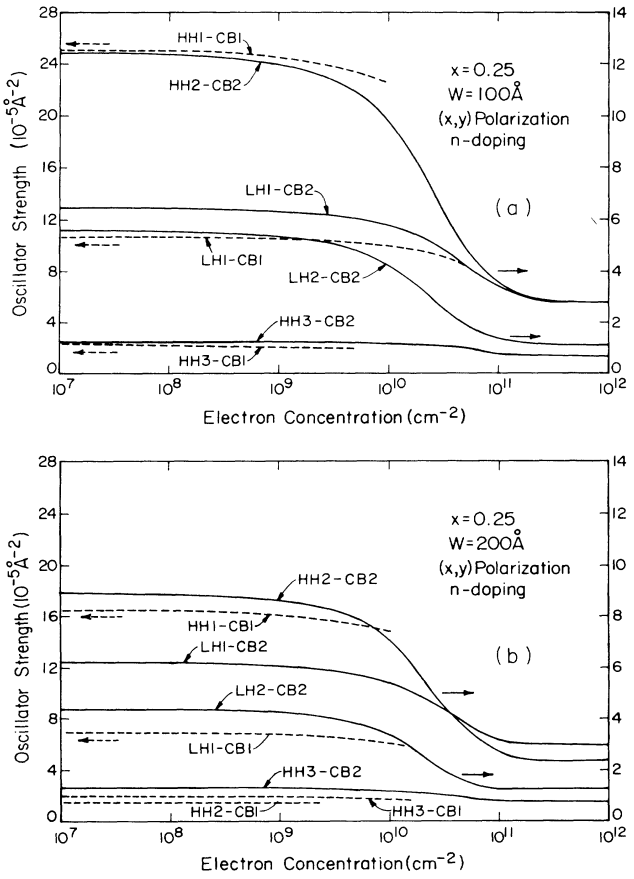

FIG. 19. Exciton oscillator strengths per unit area for several prominent excitons versus electron concentration in 100- and 200-Å modulation-doped GaAs-$Al_{0.25}Ga_{0.75}As$ quantum wells for x,y polarization. The left scale is for dashed curves only and the right scale for solid curves.

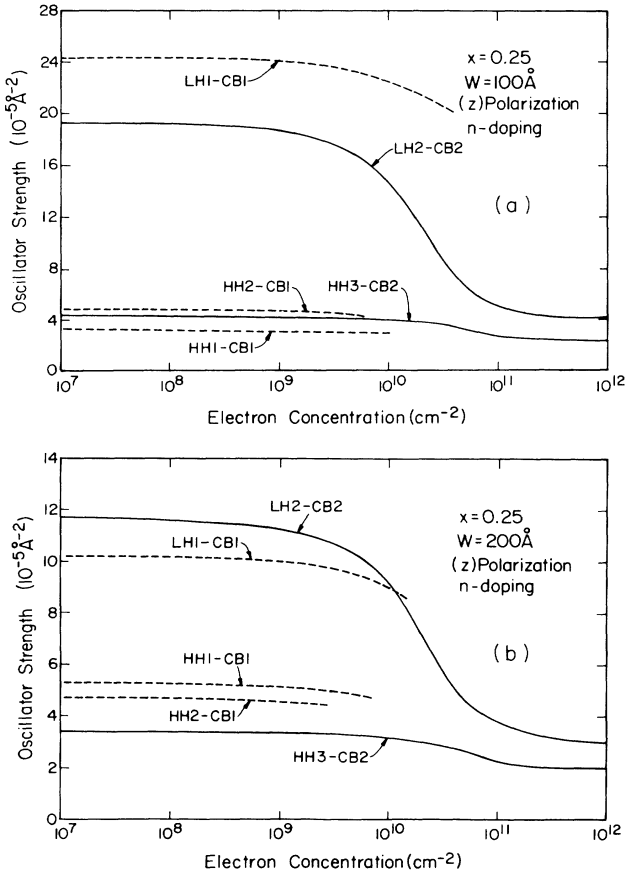

FIG. 20. Exciton oscillator strengths per unit area for several prominent excitons versus electron concentration in (a) 100- and (b) 200-Å modulation-doped GaAs-$Al_{0.25}Ga_{0.75}As$ quantum wells for z polarization. The left scale is for dashed curves only and the right scale for solid curves.

enhancement factor at intermediate doping levels. At very high doping levels the final-state interaction is completely screened, resulting in an enhancement factor of unity and in the limit of no doping and infinitely narrow wells the results of Shinada and Sugano are recovered. Our theory is compared with available experimental data and reasonable agreement between theory and experiment is found.

ACKNOWLEDGMENTS

We would like to thank J. N. Schulman, R. C. Miller, S. Lyon, and K. K. Bajaj for fruitful discussions. This work was supported by the U. S. Office of Naval Research (ONR) under Contract No. N00014-81-K-0430. The use of the computing facilities of the University of Illinois Materials Research Laboratory under the National Science Foundation (NSF) grant is gratefully acknowledged.

APPENDIX A: EXCITON EFFECTIVE-MASS EQUATION

In this appendix we derive the exciton effective-mass equations. The quantum-well conduction-band free-carrier state $|\mathbf{k}_{||},n\rangle$ is given by

$$\sum_{\sigma} f_n^{\sigma}(z_e)U(\mathbf{r})e^{i\mathbf{k}_{||}\cdot\boldsymbol{\rho}}\chi_{\sigma} ,$$

where $f_n^{\sigma}(z_e)$ is the envelope function, $U(\mathbf{r})$ is the bulk Bloch state at $\mathbf{k}=0$, χ_{σ} is the spin-wave function ($\sigma=\pm\frac{1}{2}$), and $\hat{\boldsymbol{\rho}}=x\hat{\mathbf{x}}+y\hat{\mathbf{y}}$. The subbands are indexed by n. The free-carrier state satisfies the quantum-well Schrödinger equation

$$H_e\,|\,\mathbf{k}_{||},n\,\rangle=E_n^e(\mathbf{k}_{||})\,|\,\mathbf{k}_{||},n\,\rangle .$$

The free-carrier states for holes in a quantum well are given by

$$|\,\mathbf{q}_{||},m\,\rangle=\sum_{\nu} g_m^{\nu}(\mathbf{q}_{||},z_h)U^{\nu}(\mathbf{r})e^{i\mathbf{q}_{||}\cdot\boldsymbol{\rho}} ,$$

where $g_m^{\nu}(\mathbf{q}_{||},z_h)$ is the envelope function for spin ν ($\nu=-\frac{3}{2},-\frac{1}{2},\frac{1}{2},\frac{3}{2}$), $U^{\nu}(\mathbf{r})$ is the associated bulk Bloch function, and m labels the subbands. In the quantum well we have

$$H_h\,|\,\mathbf{q}_{||},m\,\rangle=E_m^h(\mathbf{q}_{||})\,|\,\mathbf{q}_{||},m\,\rangle .$$

The noninteracting Hamiltonian $H_0=H_e+H_h$ and in the absence of electron-hole Coulomb interaction we have

$$H_0\,|\,\mathbf{k}_{||},n\,\rangle\,|\,\mathbf{q}_{||},m\,\rangle=[E_n^e(\mathbf{k}_{||})-E_m^h(\mathbf{q}_{||})]\,|\,\mathbf{k}_{||},n\,\rangle\,|\,\mathbf{q}_{||},m\,\rangle . \tag{A1}$$

The effective-mass equation for the exciton is given by $H\psi_x=E\psi_x$, where $H=H_0+V$ and V is the electron-hole Coulomb interaction. We expand the quantum-well exciton state ψ_x in terms of the noninteracting eigenstates:

$$\psi_x=\sum_{n,m}\sum_{\mathbf{k}_{||}\mathbf{q}_{||}} F_{nm}(\mathbf{k}_{||},\mathbf{q}_{||})\,|\,\mathbf{k}_{||},n\,\rangle\,|\,\mathbf{q}_{||},m\,\rangle . \tag{A2}$$

Substituting (A2) into the Schrödinger equation $H\psi_x=E\psi_x$, multiplying on the left by $\langle\mathbf{k}'_{||},m'\,|\,\langle\mathbf{q}'_{||},m'\,|$, and making use of (A1), we obtain

$$[E_n^e(\mathbf{k}_{||})-E_m^h(\mathbf{q}_{||})-E]F_{nm}(\mathbf{k}_{||},\mathbf{q}_{||})+\sum_{n',m'}\sum_{\mathbf{k}'_{||},\mathbf{q}'_{||}}\langle\mathbf{k}_{||}n,\mathbf{q}_{||}m\,|\,V\,|\,\mathbf{k}'_{||}n',\mathbf{q}'_{||}m'\rangle F_{n'm'}(\mathbf{k}'_{||},\mathbf{q}'_{||})=0 . \tag{A3}$$

We are interested in excitons at rest and so we write

$$F_{nm}(\mathbf{k}_{||},\mathbf{q}_{||})=\delta(\mathbf{k}_{||}+\mathbf{q}_{||})G_{nm}(\mathbf{k}_{||}) . \tag{A4}$$

In this case (A3) reduces to

$$[E_n^e(\mathbf{k}_{||})-E_m^h(\mathbf{k}_{||})]G_{nm}(\mathbf{k}_{||})+\sum_{n',m'}\sum_{\mathbf{k}'_{||}} V_{n'm'}^{nm}(\mathbf{k}_{||},\mathbf{k}'_{||})G_{n'm'}(\mathbf{k}_{||})=EG_{nm}(\mathbf{k}_{||}) . \tag{A5}$$

The bare electron-hole Coulomb interaction in coordinate space is given by

$$\bar{V}(\mathbf{r})=\frac{-e^2}{\epsilon_0[\rho^2+(z_e-z_h)^2]^{1/2}} . \tag{A6}$$

Taking the Fourier-Bessel transform of (A6), we have

$$\bar{v}(\mathbf{q})=\frac{-e^2}{\epsilon_0\,|\,\mathbf{q}\,|}e^{-|\,\mathbf{q}\,|\,|z_e-z_h|} \tag{A7}$$

from which we obtain the required matrix element

$$\bar{V}_{n'm'}^{nm}(\mathbf{k}_{||},\mathbf{k}'_{||})=\frac{-e^2}{\epsilon_0\,|\,\mathbf{k}_{||}-\mathbf{k}'_{||}\,|}\int\int dz_e\,dz_h\sum_{\sigma} f_{n'}^{*\sigma}(z_e)f_n^{\sigma}(z_e)\sum_{\nu} g_{m'}^{*\nu}(\mathbf{k}'_{||},z_h)g_m^{\nu}(\mathbf{k}_{||},z_h)e^{-|\,\mathbf{k}_{||}-\mathbf{k}'_{||}\,|\,|z_e-z_h|} . \tag{A8}$$

APPENDIX B: VARIATIONAL SOLUTION OF EXCITON EFFECTIVE-MASS EQUATION

The exciton envelope function $G_{nm}(\mathbf{k}_{||})$ and binding energy E_{nm} are obtained by solving the effective-mass equation

$$\sum_{\mathbf{k}'_{||}} H_{nm}(k_{||},k'_{||})G_{nm}(\mathbf{k}'_{||})=E_{nm}G_{nm}(\mathbf{k}_{||}) \tag{B1}$$

with

$$H_{nm}(\mathbf{k}_{||},\mathbf{k}'_{||})=[E_n^e(\mathbf{k}_{||})-E_m^h(\mathbf{k}_{||})]\delta_{\mathbf{k}_{||},\mathbf{k}'_{||}} + \bar{V}_{nm}(|\mathbf{k}_{||}-\mathbf{k}'_{||}|)/\epsilon(|\mathbf{k}_{||}-\mathbf{k}'_{||}|) .$$

Here $\epsilon(q)$ is the wave-vector-dependent dielectric constant described in the text, $E_n^e(\mathbf{k}_{||})$ and $E_m^h(\mathbf{k}_{||})$ are conduction and valence subbands, respectively, and the bare Coulomb potential $\bar{V}_{nm}(q_{||})$ is given by

$$\bar{V}_{nm}(q_{||})=\frac{-e^2}{q_{||}}\sum_{\sigma,\nu}\int_{-\infty}^{\infty}\int_{-\infty}^{\infty}dz_e\,dz_h\,|f_n^{\sigma}(z_e)|^2 \times |g_m^{\nu}(z_h)|^2 e^{-q_{||}|z_e-z_h|} . \tag{B2}$$

The functions $f_n^{\sigma}(z_e)$ and $g_m^{\nu}(z_h)$ are the exact zone center wave functions obtained by solving the finite square-well problem. The integral (B2) is a function of $q_{||}$ which can be performed numerically.

The exciton envelope function $G_{nm}(\mathbf{k}_{||})$ is expanded in a set of Gaussian basis functions:

$$G_{nm}(\mathbf{k}_{||})=\sum_{\beta}C_{nm}^{\beta}|\beta\rangle , \tag{B3}$$

where

$$\langle\mathbf{k}_{||}|\beta\rangle=\frac{1}{\sqrt{2\pi\beta}}\exp\left[-\frac{k_{||}^2}{4\beta}\right] . \tag{B4}$$

Here β is a set of Gaussian exponents chosen to cover a broad physical range.

The overlap integral $S(\beta,\beta')$ is given by

$$S(\beta,\beta')=\langle\beta|\beta'\rangle=\sum_{k_{||}}\langle\beta'|\mathbf{k}_{||}\rangle\langle\mathbf{k}_{||}|\beta\rangle . \tag{B5}$$

Substituting (B4) into (B5) and performing the integration, one obtains

$$S(\beta,\beta')=\frac{2\sqrt{\beta\beta'}}{\beta+\beta'} . \tag{B6}$$

The kinetic-energy matrices $T(\beta,\beta')$ are given by

$$T(\beta,\beta')=\langle\beta|E_n^e(\mathbf{k}_{||})-E_m^h(\mathbf{k}_{||})|\beta'\rangle . \tag{B7}$$

If one assumes that the energy bands are isotropic, i.e., that $E(\mathbf{k}_{||})=E(|\mathbf{k}_{||}|)$, then (B7) reduces to a one-dimensional integral which can be performed numerically. The result is given by

$$T(\beta,\beta')=\frac{1}{\sqrt{\beta\beta'}}\int_0^{\infty}dk_{||}\,E(k_{||})k_{||}\exp\left[-\frac{\beta+\beta'}{4\beta\beta'}k_{||}^2\right] , \tag{B8}$$

where $E(k_{||})=E_n^e(|k_{||}|)-E_m^h(|k_{||}|)$ depends only on $|\mathbf{k}_{||}|$.

The potential matrix element in the Gaussian basis is evaluated in coordinate space. The real-space Coulomb interaction is given by taking the Fourier-Bessel transform of (B2),

$$V_{nm}(\rho)=\int_0^{\infty}dq_{||}\,q_{||}J_0(q_{||}\rho)\bar{V}_{nm}(q_{||})/\epsilon(q_{||}) , \tag{B9}$$

where $J_0(x)$ is the zero-order Bessel function. The matrix elements are given by

$$V_{nm}(\beta,\beta')=\langle\beta|V_{nm}(\rho)|\beta'\rangle , \tag{B10}$$

where $\langle\rho|\beta\rangle=(\sqrt{2\beta/\pi})e^{-\beta\rho^2}$ is the Fourier-Bessel transform of (B4). Performing the integration over ρ one is left with a one-dimensional integral over $q_{||}$ which can be performed numerically:

$$V_{nm}(\beta,\beta')=\frac{2\sqrt{\beta\beta'}}{\beta+\beta'}\int_0^{\infty}dq_{||}\,q_{||}\frac{\bar{V}_{nm}(q_{||})}{\epsilon(q_{||})}\exp\left[\frac{-q_{||}^2}{4(\beta+\beta')}\right] .$$

*Present address: Universal Energy Systems, 4401 Dayton-Xenia Road, Dayton, OH 45432.

[1]S. Hiyamizu, J. Saito, K. Nambu, and T. Ishikawa, Jpn. J. Appl. Phys. 22, L609 (1983).
[2]J. C. M. Hwang, A. Kastalsky, H. L. Störmer, and V. G. Keramidas, Appl. Phys. Lett. 44, 802 (1984).
[3]R. Dingle, H. L. Störmer, A. C. Gossard, and W. Wiegmann, Appl. Phys. Lett. 33, 665 (1978).
[4]H. L. Störmer, A. C. Gossard, W. Wiegmann, and K. Baldwin, Appl. Phys. Lett. 39, 912 (1981).
[5]J. Klem, T. J. Drummond, R. Fischer, T. Henderson, and H. Morkoc, J. Electron. Mater. 13, 741 (1984).
[6]A. Pinczuk, J. Shah, R. C. Miller, A. C. Gossard, and W. Wiegmann, Solid State Commun. 50, 735 (1984).
[7]C. H. Yang and S. A. Lyon, Physica 134B, 305 (1985).
[8]R. C. Miller and D. A. Kleinman, J. Lumin. 30, 520 (1985).
[9]J. M. Luttinger and W. Kohn, Phys. Rev. 97, 869 (1955).
[10]J. M. Luttinger, Phys. Rev. 102, 1030 (1956).
[11]P. Lawaetz, Phys. Rev. B 4, 3460 (1971).
[12]S. S. Nedorezov, Fiz. Tverd. Tela (Leningrad) 12, 2269 (1971) [Sov. Phys.—Solid State 12, 1814 (1971)].
[13]A. Fasolino and M. Altarelli, in *Two Dimensional Systems, Heterostructures, and Superlattices*, edited by G. Bauer, F. Kuchar, and H. Heinrich (Springer, New York, 1984), p. 176; M. Altarelli, Phys. Rev. B 32, 5138 (1985).
[14]G. D. Sanders and Y.-C. Chang. Phys. Rev. B 31, 6892 (1985); J. Vac. Sci. Technol. B 3, 1285 (1985).
[15]Y.-C. Chang, Appl. Phys. Lett. 46, 710 (1985).
[16]H. J. Lee, L. Y. Juravel, J. C. Wolley, and A. J. Springthorpe, Phys. Rev. B 21, 659 (1980).

[17]R. C. Miller, A. C. Gossard, D. A. Kleinman, and D. Muntaneu, Phys. Rev. B **29**, 3470 (1984).
[18]K. Hess, D. Bimberg, L. N. Lipari, T. V. Fischbach, and M. Altarelli, in *Proceedings of the 13th International Conference on the Physics of Semiconductors, Rome, Italy, 1976,* edited by F. G. Iurmi (North-Holland, Amsterdam, 1976), p. 142.
[19]See, for example, K. Ploog, in *Two-dimensional System, Heterostructures, and Superlattices,* edited by G. Bauer, F. Kuchar, and H. Heinrich (Springer, New York, 1984), p. 220; P. Ruden and G. H. Dohler, Phys. Rev. B **27**, 3538 (1983).
[20]R. Dingle, in *Festkörperprobleme, Advances in Solid State Physics,* edited by H. J. Queisser (Pergamon/Vieweg, Braunschweig, 1975), Vol. VX, p. 21.
[21]A. C. Gossard, *Treatise on Materials Science and Technology,* edited by K. T. Tu and R. Rosenberg (Academic, New York, 1982), Vol. 24.
[22]R. L. Greene and K. K. Bajaj, Solid State Commun. **45**, 9, 831 (1983); J. Vac. Sci. Technol. B **1**, 391 (1983).
[23]C. Priester, G. Allen, and M. Lannoo, Phys. Rev. B. **30**, 12 (1984); **30**, 7302 (1984).
[24]D. A. Kleinman, Phys. Rev. B **32**, 3766 (1985).
[25]Y.-C. Chang and J. N. Schulman, Appl. Phys. Lett. **43**, 536 (1983); Phys. Rev. B **31**, 2069 (1985).
[26]G. D. Sanders and Y.-C. Chang, Phys. Rev. B **32**, 4282 (1985).
[27]G. D. Mahan, Phys. Rev. **153**, 882 (1967).
[28]Y.-C. Chang and G. D. Sanders, Phys. Rev. B **32**, 5521 (1985).
[29]U. Fano, Phys. Rev. **124**, 1866 (1961).
[30]P. J. Price, J. Vac. Sci. Technol. **19**, 599 (1981).
[31]I. S. Gradshteyn and I. M. Ryzhik, *Table of Integrals, Series and Products* (Academic, New York, 1980), p. 685.
[32]F. Stern, Phys. Rev. Lett. **18**, 546 (1967).
[33]J. A. Brum, G. Bastand, and C. Guillemot, Phys. Rev. B **30**, 905 (1984).
[34]Y.-C. Chang, J. Appl. Phys. **59**, 2173 (1986).
[35]G. D. Sanders and Y.-C. Chang, Phys. Rev. B **32**, 5517 (1985).
[36]See, for example, F. Bassani and C. P. Parrasvacini, *Electronic States and Optical Properties in Solids* (Pergamon, New York, 1975).
[37]K. B. Kahen and J. P. Leburton, Appl. Phys. Lett. **47**, 508 (1985).
[38]H. Yamamoto, M. Asada, and Y. Suematsu, Electron. Lett. **21**, 5791 (1985).
[39]M. Shinada and S. Sugano, J. Phys. Soc. Jpn. **21**, 1936 (1966).
[40]R. C. Miller, A. C. Gossard, G. D. Sanders, Y.-C. Chang, and J. N. Schulman, Phys. Rev. B **32**, 8452 (1985).
[41]W. T. Masselink, P. J. Pearah, J. Klem, C. K. Peng, H. Morkoc, G. D. Sanders, and Y.-C. Chang, Phys. Rev. B **32**, 8027 (1985).
[42]We would also like to correct an error in Fig. 3(b) of Ref. 14. In this figure the energy axis should be rigidly shifted by 28 meV toward the lower-energy side; the spectrum remains unchanged.
[43]E. Burstein, Phys. Rev. **93**, 632 (1954); T. S. Moss, Proc. Phys. Soc. London, Sect. B **67**, 755 (1954).